Genomic Insights into a Multispecies Bacterial Pathogen Complex Driving Bacterial Blotch in White Button Mushrooms.

Sameerika D Mudiyanselage[1], Michelle Lee[1], Jose C. Huguet-Tapia[1], Romina Gazis[2*], Samuel J Martins[1*].

[1]Department of Plant Pathology, University of Florida, Gainesville, FL, 32611, USA.

[2]Department of Plant Pathology, Tropical Research Education Center, Homestead. FL, 33031-3314, USA.

*Correspondence:

Samuel J Martins

Department of Plant Pathology

University of Florida

2413 Fifield Hall

2550 Hull Road

Gainesville, FL, 32611

Email: sj.martins@ufl.edu

Romina Gazis

Department of Plant Pathology

UF/IFAS TREC

18905 SW 280 St.

Homestead, FL 33031-3314

Email: r.gazisseregina@ufl.edu

ABSTRACT

Bacterial blotch remains a major constraint to global white button mushroom (*Agaricus bisporus*) industry, yet its etiological complexity has been underestimated. Through a genome resolved, polyphasic approach applied to symptomatic mushrooms collected from United States, we uncovered an unexpectedly diverse complex of *Pseudomonas* species driving blotch disease. Beyond classical pathogens (*P. tolaasii*, *P. gingeri*, *P. agarici*, and *P.* "*reactans*", *P. yamanorum*, *Pseudomonas* sp. NC02), our analyses revealed a striking prevalence of *P. azotoformans*, a species not previously associated with mushroom pathology, alongside *P. pergaminensis*, *P. monsensis*, *P. tensinigenes*, *P. simiae*, *Pseudomonas* sp. Irchel 3A7, *Pseudomonas* sp. REP124 and two putatively novel lineages. Comparative genomics demonstrated pronounced heterogeneity in accessory genome content, with *P. azotoformans* exhibiting exceptional genomic plasticity indicative of broad ecological adaptability. Secondary metabolite profiling and white line assays further delineated species-specific chemotaxonomic signatures, underscoring the multifactorial nature of virulence. Collectively, this study provides the most comprehensive genomic and phenotypic characterization of blotch-associated *Pseudomonas* in Northern America, overturning the long-held paradigm of a single dominant pathogen. By establishing that bacterial blotch is multispecies disease complex, our findings redefine its epidemiology and lay the foundation for improved diagnostics strategies in mushroom production systems. The emergence and high prevalence of *P. azotoformans* underscore the limitations of diagnostic protocols focused exclusively on classical blotch pathogens and highlight the need for broader, genomics informed detection strategies. Collectively, this work offers actionable insights to strengthen production resilience and support the sustainability of white button mushroom cultivation as the world's most economically important specialty food crop.

Keywords: *Agaricus bisporus*, *Pseudomonas azotoformans*, Multilocus sequence analysis, Average nucleotide identity, Whole genome sequencing

1. INTRODUCTION

The white button mushroom (*A. bisporus*) is one of the fastest growing and most widely cultivated mushroom species globally, with major production hubs in China, the United States, the Netherlands, Poland, Italy, and India. In the United States alone, white button mushrooms represent over 90% of total mushroom consumption underscoring their central role in the national and global mushroom markets (Royse et al., 2017). Beyond its economic importance, *A. bisporus* is a nutritionally dense functional food, providing high-quality proteins, carbohydrates, essential vitamins, minerals and dietary fibers (Atila et al., 2017). It also produces a diverse array of bioactive compounds, including polysaccharides, phenolics, flavonoids, and terpenoids, which exhibit antioxidant, anti-inflammatory, anti-aging, immunomodulatory properties. These compounds have been linked to numerous health benefits, including the reduction of chronic disease risk and cancer prevention (Zhang et al., 2024; Li et al., 2025). Consequently, these combined nutritional and medicinal attributes establish *A. bisporus* as both a staple crop and a critical source of therapeutic compounds. Despite these benefits the commercial production of *A. bisporus* faces a significant and persistent threat from "bacterial blotch", one of the most destructive postharvest diseases affecting *A. bisporus,* which has impacted commercial production worldwide for decades (Osdaghi et al., 2019; Soler-Rivas et al., 1999).

Bacterial blotch is primarily associated with *Pseudomonas* species, metabolically versatile and ubiquitous bacteria that naturally inhabit the casing layer. Some *Pseudomonas* strains, such as *P. putida* (Eger, 1972) and *P. poae* n12 (Fermor et al., 2000), play beneficial roles in mushroom cultivation promoting *A. bisporus* growth and contributing to primordia formation. However, pathogenic *Pseudomonas* species often persist in casing materials even after pasteurization, leading to disease outbreaks. The bacterial blotch disease is characterized by rapid discoloration of the mushroom cap, pitting, tissue degradation, and, ultimately, extensive postharvest losses. Different blotch phenotypes correspond to different pathogens: *P. tolaasii* causes brown blotch, producing sunken greenish-brown lesions that expand and coalesce (Soler-Rivas et al. 1999), while *P. gingeri* causes ginger blotch, marked by golden-yellow discoloration (Wong and Fletcher, 1979). Beyond these well-known species, few surveys have revealed a much broader diversity of blotch-causing

91 bacteria, including *P. agarici* (Fatmi et al., 2008, Geels et al., 1994; Young, 1970), *P.*
92 "*reactans*" (Wells et al., 1996), *Pseudomonas* sp. NZ17P (Godfrey et al., 2001), *P*
93 *costantinii* (Munch et al., 2000; Taparia et al., 2020), *P. yamanorum*, *P. edaphica*, *P.*
94 *salomonii*, *Pseudomonas* sp. NC02 (Taparia et al. 2020), and *P. extremorientalis* (Huang
95 et al. 2026). A few non-*Pseudomonas* species have been reported in the years to cause
96 blotch-like symptoms, which include *Mycetocola* sp. (Hamidizade et al. 2020), *Serratia*
97 *liquefaciens*, *S. proteamaculans*, *Pantoea* sp. (Taparia et al. 2020), and *Cedecea neteri*
98 (Huang et al. 2024), highlighting the increasing complexity of this disease.
99 Pathogenic *Pseudomonas* species employ multiple virulence mechanisms, including
100 extracellular proteases and lipases (Morihara and Homma, 1985), antifungal metabolites
101 (Henkels et al. 2014), and cyclic lipopeptides (CLPs) that enhance motility, surface
102 colonization, competition, and infection. In addition to pathogen-derived factors, the
103 development of blotch symptoms is influenced by the mushroom's physiological
104 responses, particularly enhanced tyrosinase activity and increased phenolic content, which
105 collectively accelerate browning and tissue discoloration (Soler-Rivas et al. 1999).
106 Historically, the identification of bacterial blotch-causing *Pseudomonas* species has relied
107 heavily on phenotypic assays such as the White Line Agar Assay (WLA), which detects
108 the interaction between tolaasin produced by *P. tolaasii* and the WLIP compound produced
109 by the organism described as *P. reactans*. However, the increasing diversity of blotch-
110 causing *Pseudomonas* species and the frequent inconsistency of WLA results have made it
111 clear that phenotypic tests alone are insufficient for accurate species identification.
112 Although multilocus sequence analysis (MLSA) and 16S rRNA-based approaches have
113 been widely used for *Pseudomonas* taxonomy, several studies have demonstrated their
114 limitations, particularly in resolving closely related taxa (Gomila et al. 2015).
115 Consequently, modern polyphasic strategies that combine MLSA, whole-genome
116 comparisons, and chemotaxonomic profiling now provide the most robust framework for
117 species-level resolution within the genus *Pseudomonas*.
118 Despite decades of research, the complete and accurate diversity of blotch-causing
119 *Pseudomonas* species remains unresolved, highlighting the urgent need for broader surveys
120 that address both identification and management, as effective control strategies depend on

121 precise pathogen recognition. This growing complexity underscores the importance of
122 region-specific assessments of pathogen diversity. In this study, we conducted a systematic
123 survey of symptomatic white button mushrooms collected from two commercial
124 production sites in the United States. Specifically, we aimed to characterize the causative
125 agents of bacterial blotch by integrating phenotypic assays (WLA and fluorescence),
126 pathogenicity tests, MLSA, whole-genome analyses, comparative genomics, and *in silico*
127 profiling of secondary metabolite biosynthetic gene clusters. Together, these approaches
128 provided a comprehensive overview of the bacterial blotch pathogens present in these
129 production systems and their associated dynamics on *Agaricus bisporus.*
130

131 **2. MATERIALS AND METHODS**

132 **2.1. Isolation of *Pseudomonas* sp. from white button mushrooms**

133 White button mushrooms displaying bacterial blotch symptoms were collected between
134 April and May 2025 from two major commercial mushroom production companies in the
135 United States. These companies represent large-scale, vertically integrated production
136 systems operating multiple geographically distributed facilities. For this study, samples
137 were collected from one farm located in the southern United States from each supplier,
138 hereafter referred to as Farm X and Farm Y.
139 At Farm X, sampling was conducted during the second and third production flushes,
140 whereas at Farm Y, sampling occurred during the first flush. At the time of collection,
141 disease incidence was substantially higher at Farm X (approximately 30%) compared to
142 Farm Y (1–2%). Symptomatic mushrooms were transported to the laboratory under cold
143 conditions in individual ziplock bags, and bacterial isolation was conducted within 24 to
144 48 h of arrival. Upon arrival, the mushrooms were gently rinsed with sterile distilled water
145 to remove surface debris. Approximately 1 cm^2 of tissue was excised from the margin
146 between diseased and healthy areas using a sterile scalpel. Each tissue sample was
147 transferred into a microcentrifuge tube containing 1 mL of 10% sodium hypochlorite
148 (NaOCl), vortexed for 2 s, and allowed to stand at room temperature for 30 s for surface
149 disinfection. The samples were subsequently rinsed twice with 1 mL of sterile distilled
150 water, briefly vortexing after each rinse. The disinfected tissue was then macerated in 100

151 µL of 0.01 M sterile phosphate buffer (pH 7.0) using a sterile disposable pestle, and the
152 homogenate was vortexed to ensure a uniform suspension. Serial dilutions were prepared,
153 and a 10 µL aliquot from each dilution was streaked onto King's B (KB) (King et al., 1954)
154 agar plates, supplemented with novobiocin (45 µg mL^{-1}), penicillin (75 units mL^{-1}), and
155 cycloheximide (75 µg mL^{-1}) (Suyama et al., 2000). As a control, isolation was also
156 performed from one asymptomatic mushroom collected at each site. All plates were
157 incubated at 27°C for 48 h to allow for bacterial growth. Morphologically distinct bacterial
158 colonies were re-streaked onto freshly prepared KB plates until pure single-colony isolates
159 were obtained. Pure cultures were preserved in 50% glycerol at -80°C for subsequent
160 analyses.
161
162 **2.2. Genomic fingerprinting of bacterial isolates**
163 A total of 76 bacterial isolates were selected for BOX-PCR fingerprinting to assess genetic
164 diversity and identify representative isolates for subsequent analyses. A single colony from
165 each isolate was suspended in 50 µL of sterile distilled water, heated at 95°C for 10 min to
166 lyse the cells, immediately chilled on ice for 2 min, and centrifuged at 12,000 × g for 5 min
167 to pellet cell debris. One microliter of the supernatant was used directly as the DNA
168 template for BOX-PCR amplification using the BOXA1R primer (5′-
169 CTACGGCAAGGCGACGCTGACG-3′), following a modified protocol by Rademaker et
170 al. (1998). The PCR reaction mixture contained 1× Green GoTaq buffer,
171 0.08 mg mL^{-1} BSA (NEB), 10% DMSO, 1.25 mM dNTPs, 1.76 µM BOXA1R primer, 1.25
172 U GoTaq G2 DNA polymerase (Promega), and 1 µL of DNA template, for a total volume
173 of 25 µL. PCR amplification was performed in an Applied Biosystems Veriti 96-well
174 thermal cycler with the following cycling conditions: initial denaturation at 95°C for 2 min;
175 29 cycles of 94°C for 3 s, 92°C for 30 s, 50°C for 1 min, and 65°C for 8 min; followed by
176 a final extension at 65°C for 8 min. Amplified products were separated by electrophoresis
177 on 1.5% (w/v) molecular-grade agarose gels in 0.5× TAE buffer (Quality Biological) at 60
178 V and 30 mA for 16 h at 4°C. The gels were visualized, and banding patterns were captured
179 using the Biorad gel doc XR imaging system. DNA fingerprint profiles were further
180 analyzed using ImageJ (Sánchez-Jaramillo et al., 2022) for pattern recognition and

181 assessment. Pairwise dissimilarities among isolates were calculated using Jaccard's
182 distance (Jaccard, 1908), and hierarchical clustering was performed with the unweighted
183 pair group method with arithmetic mean (UPGMA) (Sokal and Sneath, 1963) using R
184 software (v4.4.1). Clusters were defined at a 90% similarity threshold, and a binary
185 heatmap was generated to visualize variation in band distribution among isolates.
186
187 **2.3. Pathogenicity Assay**
188 Based on the genetic dissimilarity analysis, 61 isolates were selected for *in vitro*
189 pathogenicity testing. Bacterial suspensions for inoculation were prepared from 5 mL
190 overnight cultures grown in KB broth at 27°C with shaking at 120 rpm for 24 h. The
191 cultures were centrifuged at 8,000 rpm for 10 min, and the resulting cell pellets were
192 washed once with 0.01 mM phosphate-buffered saline (PBS), followed by centrifugation.
193 The cells were resuspended in the same buffer, and the optical density at 600 nm (OD_{600})
194 was adjusted to 0.5 using a Bio-Rad SmartSpec™ 3000 spectrophotometer, corresponding
195 to approximately 10^9 colony-forming units (CFU) per mL. *Pseudomonas protegens*
196 BP1304 and *Pseudomonas tolaasii* BP1106 were used as negative and positive controls,
197 respectively. Pathogenicity assays were performed on fresh, healthy white button
198 mushrooms obtained from a local market. To maintain high humidity, sterile plastic trays
199 were lined with moist filter paper. The mushroom caps were surface sterilized by
200 immersion in 10% sodium hypochlorite (NaOCl) for 30 s, rinsed twice with sterile distilled
201 water, and air-dried under sterile conditions. The stalks were removed, and the epidermal
202 layer of the cap surface was peeled away to expose the inner tissue. Caps were then cut
203 into uniform cubes (4 cm × 2 cm) using sterile scalpels, and each cube was placed
204 individually in a sterile petri dish to prevent cross-contamination. Three inoculation sites
205 were designated on each cube using a sterile No. 4 cork borer (4 mm diameter) to mark
206 circular areas, following Henkels et al. (2014). A 10 μL aliquot of bacterial suspension was
207 applied to each marked site. For each isolate, nine replicate mushroom cubes were tested,
208 and the entire assay was independently repeated three times. Petri dishes containing the
209 mushroom cubes were sealed and incubated in the dark at 27°C for three days. Symptom
210 development was monitored and photographed daily to assess tissue maceration, pitting,

211 or discoloration until 72 h. Severity scores were assigned as follows: 1= mild or slow
212 discoloration; 2= rapid tissue discoloration without tissue pitting; 3= extensive
213 discoloration accompanied by tissue pitting.
214
215 **2.4. Florescence and White Line Agar (WLA) test**
216 All isolates (*n* = 61) were cultured on KB medium, and their ability to produce fluorescent
217 pyoverdine and related metabolites was evaluated under UV light (365 nm) after 48 h of
218 incubation. The white line reaction assay was performed to assess the production of
219 extracellular lipopeptides, including tolaasin and WLIP (white line inducing principle),
220 following the methods described by Osdaghi et al. (2019). Briefly, *P. fluorescens* Pf-5P
221 was streaked against each isolate to evaluate tolaasin production, while *Pseudomonas*
222 *tolaasii* BP1106 was used to assess the secretion of WLIP and related lipopeptides. On
223 King's B agar, two loopfuls of each test isolate were streaked approximately 8 mm from
224 the reference strain. Plates were incubated at 27 °C, and white-line formation was
225 monitored over a 72 h period. A positive white-line reaction was defined as the formation
226 of a distinct white precipitate at the interface between the test isolate and either
227 *Pseudomonas fluorescens* Pf-5 or *P. tolaasii* BP1106.
228
229 **2.5. DNA extraction and Whole Genome Sequencing**
230 Genomic DNA from the (*n* = 61) isolates was extracted using the Quick-DNA Fecal/Soil
231 Microbe MiniPrep Kit (Zymo Research). The quality and concentration of the DNA were
232 verified using a Bio-Rad Universal Hood Gel Doc XR UV Transilluminator (200 VA)
233 system, and quantity was evaluated using Nanodrop spectrophotometer (Thermo Fisher
234 Scientific). Whole-genome sequencing was performed by SeqCenter (Pittsburgh).
235 Sequencing libraries were constructed using the Illumina DNA Prep Kit (tagmentation-
236 based) with custom IDT 10-bp unique dual indices (UDI) and an average insert size of
237 approximately 280 bp. Paired-end sequencing (2 × 151 bp) was conducted on an Illumina
238 NovaSeq X Plus platform. Raw read demultiplexing, adapter removal, and initial quality
239 control were performed using bcl-convert (v4.2.4).
240

241 **2.6. Genome assembly**

242 The quality of the reads was assessed with FastQC (v0.12.1) (Chen et al., 2018). Based on
243 the quality metrics, low-quality bases and residual adapter sequences were trimmed using
244 Trim Galore (v0.6.10), applying a Phred quality cutoff of 20. To remove potential primer
245 or adapter contamination, 15 bases were clipped from the 5′ ends and 10 bases from the 3′
246 ends of both forward and reverse reads. Paired reads that passed all quality filters were
247 retained for downstream analyses. High-quality reads were assembled de novo using
248 SPAdes (v4.0.0) (Bankevich et al., 2012), and contigs shorter than 500 bp and a K-mer
249 coverage of less than 2.0 were filtered out. Assembly quality was evaluated with QUAST
250 (v5.2.0) (Gurevich et al., 2013), and genome completeness was estimated using BUSCO
251 (v5.8.3) based on lineage-specific single-copy orthologs (Simão et al., 2015). Only
252 *Pseudomonas* strains ($n = 57$) were used for downstream analysis. Assembled genomes for
253 all 57 strains were submitted to NCBI under Bio Project PRJNA1377199, with accession
254 numbers SAMN53759319 to SAMN53759375.

255

256 **2.7. Genome-wide comparisons**

257 The identity of each isolate was determined using data from assembled genome sequences
258 submitted to the Type (Strain) Genome Server TYGS, (https://tygs.dsmz.de) for whole-
259 genome-based taxonomic analysis(Meier-Kolthoff and Göker, 2019; Meier-Kolthoff et al.,
260 2013). TYGS calculates digital DNA–DNA hybridization (dDDH) values using multiple
261 formulas, including dDDH4, which estimates nucleotide identity within high-scoring
262 genome alignments. A dDDH4 value above 70% is used for taxonomic delineation (Meier-
263 Kolthoff et al., 2013). For further classification, the Average Nucleotide Identity (ANI)
264 based Genome Taxonomy Database classify workflow GTDB-Tk (v2.4.1) (Chaumeil et
265 al., 2022) was used with a threshold of 95% to determine species boundaries. TYGS and
266 GTDB-Tk were also used to identify the closest relative strains, including type strains, for
267 comparative analysis. Pairwise ANI values of the isolates and their closest relatives were
268 computed using all-versus-all strategies with FastANI (v1.34) (Dataset S02) (Jain et al.,
269 2018). ANI similarity values greater than 95% were used to construct a phylogenetic
270 heatmap in RStudio using the pheatmap package (v1.0.13). When the above methods were

271 insufficient to confidently resolve species-level identity, we further assessed genomic
272 relatedness using the Genome-to-Genome Distance Calculator (GGDC)
273 (https://ggdc.dsmz.de/ggdc.php) (Meier-Kolthoff et al., 2022).
274 Multi-locus sequence analysis (MLSA) was performed to infer the evolutionary history of
275 the bacterial genomes using eight conserved housekeeping genes (*rpoD, rpoB, recA, gapA,*
276 *gltA, atpD, gyrB,* and *ileS*) from nine reference strains (Dataset S01). A total of 31 closely
277 related reference sequences, including *Pseudomonas lurida* LMG21995^T as the outgroup,
278 were retrieved from NCBI and included in the phylogenetic analysis (Dataset S01).
279 Reference strains included all available type strains unless otherwise noted. Type strain
280 names were confirmed with The List of Prokaryotic names with Standing in Nomenclature
281 (LPSN) (Parte et al., 2020). Gene sequences were extracted and aligned using AutoMLSA2
282 (v2.0.9.0) (https://github.com/davised/automlsa2), which features an automated pipeline
283 that identifies housekeeping genes, performs multiple sequence alignment using MAFFT
284 (v7.520), and concatenates the alignments. The concatenated alignment totaled 176,583
285 bp and was used to generate a maximum-likelihood phylogenetic tree using IQ-TREE
286 (v3.0.1) with node support values based on 1,000 bootstraps (Wong et al., 2025, Minh et
287 al., 2020). The phylogenetic tree was visualized using iTOL (v7.2.2) (Letunic et al., 2024).
288

289 **2.8. Core and Pan genome analysis**

290 Pan-genome analysis was performed on all 57 *Pseudomonas* isolates, without
291 incorporating external NCBI reference genomes. Additionally, for the four most abundant
292 species *P. tolaasii*, *P. gingeri*, *P. azotoformans*, and *P. pergaminensis* pan-genome and
293 core-genome profiles were constructed by integrating corresponding NCBI reference
294 genomes. All the NCBI reference accessions are listed in Dataset S01. Gene prediction and
295 functional annotation were performed with Prokka v1.14.6 (Seemann, 2014) with default
296 parameters. The resulting GFF files were used for the pan-genome analysis with Roary
297 v3.13.0 (Page et al., 2015), applying a minimum BLASTp identity of 90% for both species
298 cluster analyses and for all strains. For each species group, maximum-likelihood
299 phylogenetic analysis was conducted using RAxML v8.2.10 based on the concatenated
300 core-gene alignments generated by Roary. This analysis employed the GTR+GAMMA

301 substitution model with rapid bootstrap searches, with 100 bootstrap replicates to identify
302 the best-scoring tree (Stamatakis, 2014). Phylogenetic trees were visualized and annotated
303 in iTOL (v7.2.2). Both the resulting tree and gene presence/absence matrices were explored
304 and visualized using Phandango (Hadfield et al., 2018).
305

306 **2.9. Secondary metabolite prediction**

307 Secondary metabolite biosynthetic gene clusters (BGCs) were identified using antiSMASH
308 v7.0.0 (Blin et al., 2023) with default parameters. To focus on conserved clusters, only
309 BGCs with over 30% sequence similarity were retained for further analysis. The resulting
310 BGC profiles were compiled for all isolates, and the presence or absence of each predicted
311 cluster type was visualized in R (v4.4.1) using ggplot2 to compare secondary metabolite
312 cluster distributions among the species groups.
313

314 **3. RESULTS**

315 **3.1. Isolation of *Pseudomonas* spp. from white button mushrooms**

316 During the mushroom survey, we collected 28 symptomatic white button mushrooms from
317 Farm X and 17 from farm Y, both exhibiting typical bacterial blotch symptoms. The
318 symptoms varied in severity, ranging from light yellow, known as "ginger blotch", to dark
319 brown or chocolate-colored lesions referred to as "brown blotch". These symptoms were
320 often accompanied by sunken, water-soaked areas and collapse of the wet tissue (Fig. 1A).
321 A total of 76 bacterial isolates were selectively recovered from the samples using NCP-KB
322 medium and were used for subsequent analyses.
323 To identify isogenic strains prior to further genomic and phenotypic characterization,
324 BOX-PCR fingerprinting was performed on the 76 bacterial isolates recovered from the
325 symptomatic mushrooms. The BOX-PCR profiles exhibited banding patterns in agarose
326 gel ranging from <0.5 kb to approximately 10 kb. A binary data matrix representing the
327 presence or absence of 23 distinct BOX-PCR bands was generated and subjected to
328 clustering analysis. The resulting dendrogram (Supplementary Fig. S1) revealed 60 isolate
329 groups at a 90% similarity threshold, representing 76 distinct isolates with varying degrees
330 of relatedness. This clustering pattern demonstrated a high level of genetic diversity among

331 the isolates while also identifying 10 groups of closely related strains (isolate group 8, 14,
332 18, 23, 26, 37, 39, 40, 57, and 58). Based on these DNA fingerprint patterns, 15 isolates
333 exhibiting identical BOX-PCR profiles were considered isogenic and excluded from
334 subsequent analyses.
335
336 **3.2. Pathogenicity Assay**
337 The ability of each isolate to cause bacterial blotch symptoms was assessed *in vitro* by
338 inoculating fresh mushroom tissue cubes with each of the 61 selected isolates from the
339 BOX-PCR profiles. In this study, pathogenicity was defined as the ability to induce
340 discoloration on mushroom tissue within 2 days post-inoculation, in contrast to the
341 controls. A total of 85% of the strains were identified as producing extensive discoloration
342 accompanied by tissue pitting. An additional 7% of isolates produced only rapid tissue
343 discoloration without tissue pitting, while 8% exhibited only mild or slow discoloration,
344 comparable to the nonpathogenic control strains *Pseudomonas protegens* BP1304 and
345 *Pseudomonas tolaasii* BP1106 within 48 h post-inoculation (Table 1).
346
347 **3.3. Evaluating the potential for lipopeptide and fluorescent pigment production**
348 Among the 61 bacterial isolates examined, eight produced a white-line reaction when
349 confronted with *Pseudomonas fluorescens* Pf-5, indicating the presence of tolaasin-like
350 lipopeptides typically associated with *P. tolaasii* or closely related species. In contrast,
351 twenty-four isolates formed a distinct white line when challenged with *P. tolaasii* BP1106,
352 consistent with the production of WLIP or WLIP-like noncanonical lipopeptides. The
353 remaining 29 isolates showed no reaction with either *P. fluorescens* Pf5 or *P. tolaasii*
354 BP1106 (Table 1, Fig. 1B). Nearly all isolates exhibited fluorescence under UV
355 illumination (365 nm), indicative of pyoverdine production, except for two isolates
356 (SM395 and SM405), which did not fluoresce (Table 1).
357
358
359
360

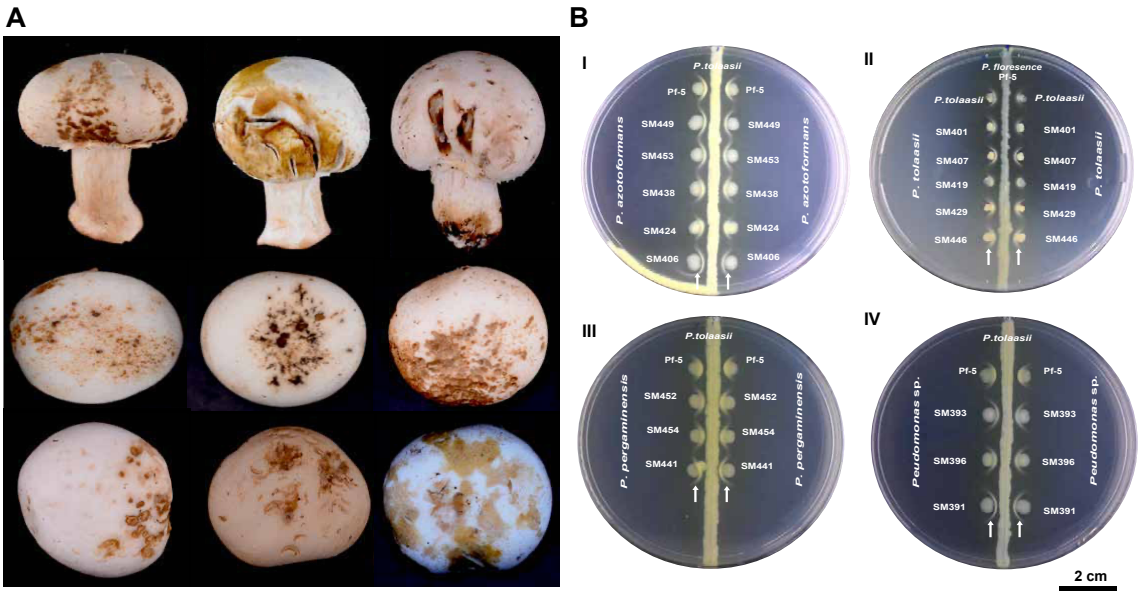

Fig. 1. Phenotypic characterization of bacterial blotch pathogens from white button mushroom collected at two U.S. farms (X and Y) in the U.S. (A) Representative blotch symptoms on mushroom caps, ranging from brown to ginger discoloration with varying degrees of tissue pitting. (B) White-line reaction assays illustrating lipopeptide-mediated interactions among *Pseudomonas* isolates: B(I) *P. azotoformans* versus *P. tolaasii* BP1106*;* B(II) *P. tolaasii* isolates versus *P. fluorescens* Pf-5*;* B(III) *P. pergaminensis* isolates versus *P. tolaasii* BP1106; B(IV) isolates SM391, SM393, and SM396 versus *P. tolaasii* BP1106. Arrows highlight distinct white precipitates, indicating positive interactions associated with cyclic lipopeptide production. Scale bar = 2 cm.

Table 1. Phenotypic characterization of isolates based on pathogenicity, white-line agar Assay (WLA), and fluorescence production.

Isolates	Pathogenicity Score*	White Line Agar Assay (WLA)†		Florescence under UV‡
		P. fluorescens Pf5	*P. tolaasii BP1106*	
SM405	1	0	0	N
SM432	3	0	0	Y
SM395	1	0	0	N
SM445	3	0	1	Y
SM434	3	0	0	Y
SM421	3	0	0	Y
SM402	3	0	1	Y
SM453	3	0	1	Y
SM439	3	0	0	Y
SM416	3	0	0	Y
SM451	3	0	1	Y
SM411	3	0	0	Y
SM438	3	0	1	Y
SM433	3	0	0	Y
SM410	3	0	0	Y
SM399	3	0	0	Y
SM428	3	0	0	Y
SM396	3	0	1	Y
SM408	3	0	1	Y
SM442	3	0	0	Y
SM436	3	0	1	Y

SM424	3	0	1	Y
SM392	3	0	0	Y
SM448	1	0	0	Y
SM449	3	0	1	Y
SM417	2	0	0	Y
SM391	3	0	1	Y
SM400	1	0	0	Y
SM393	3	0	1	Y
SM444	3	0	1	Y
SM401	3	1	0	Y
SM403	3	1	0	Y
SM409	3	0	0	Y
SM431	3	0	0	Y
SM423	3	0	1	Y
SM404	3	0	0	Y
SM406	3	0	1	Y
SM390	3	0	0	Y
SM397	3	0	0	Y
SM446	3	1	0	Y
SM437	3	1	0	Y
SM450	3	0	1	Y
SM419	3	1	0	Y
SM407	3	1	0	Y
SM441	3	0	1	Y
SM418	3	0	1	Y
SM394	3	0	1	Y
SM429	3	1	0	Y
SM454	3	0	1	Y
SM398	3	0	1	Y
SM452	3	0	1	Y
SM413	3	0	1	Y
SM447	2	0	1	Y
SM420	3	0	0	Y
SM415	2	0	0	Y
SM425	3	0	0	Y
SM426	1	0	0	Y
SM440	3	0	0	Y
SM422	3	0	0	Y
SM412	3	0	0	Y
SM430	2	1	0	Y

*Pathogenicity Score, 1= mild or slow discoloration; 2= rapid tissue discoloration without tissue pitting; 3= extensive discoloration accompanied by tissue pitting.
†White line Agar Assay, 1= presence; 0= White line absence
‡Florescence under UV, Y= Florescence; N= non-florescence

3.4. Whole genome sequencing of *Pseudomonas* isolates

We analyzed the whole genomes of 57 pathogenic *Pseudomonas* strains isolated from *Agaricus bisporus*. Illumina paired-end sequencing produced an average of 1.77 million read pairs per genome, with a range of 1.0 to 3.4 million. Over 95% of bases exceeded a Phred quality score of Q30. De novo assemblies yielded an average of 185 contigs per genome, with a mean total length of 6.77 Mb, N50 values averaging 96,095 bp, and a GC content of 61%. BUSCO analysis indicated an average genome completeness of 98%, with no detected genome duplication, fragmentation, or missing regions, ensuring high-quality data suitable for genome assembly and downstream analyses. Dataset S02 provides summary statistics of the assembly.

390

391 **3.5. Genome-wide comparison and Taxonomic classification**

392 To ensure accurate taxonomic classification and avoid potential misidentifications
393 associated with conventional methods, we employed a polyphasic approach that integrates
394 several complementary analyses. The *Pseudomonas* isolates were first evaluated using the
395 Genome Taxonomy Database Toolkit (GTDB-Tk) and the Type Strain Genome Server
396 (TYGS) for whole-genome-based taxonomic assignment. Additionally, we performed
397 multilocus sequence analysis (MLSA) of 8 conserved housekeeping genes and FastANI-
398 based average nucleotide identity comparisons to confirm species-level classifications.
399 This integrated approach provided a highly reliable and comprehensive strategy for
400 resolving taxonomic relationships within the *Pseudomonas* genus.

401 We initially used GTDB-Tk for whole-genome classification, relying on GTDB-Tk-based
402 ANI measurements to achieve high-resolution species-level assignments of the isolates.
403 We identified *Pseudomonas "gingeri*" (*n* = 11), *P. azotoformans* (*n* = 10), *P. tolaasii* (*n* =
404 7), *P. pergaminensis* (*n* = 6), and *Pseudomonas "reactans"* (*n* = 2), as well as single
405 isolates of *P. agarici, P. simiae, P. monsensis, P. yamanorum*, and *P. tensinigenes*. A
406 species boundary of >95% ANI and <83% for interspecies divergence was adopted. Isolate
407 SM400 shared 94% GTDB-Tk-based ANI with *P. allokribbensis*, while SM426 exhibited
408 90% ANI with *P. azerbaijanoccidens*, indicating low relatedness. In total, 14 isolates could
409 not be confidently assigned to any *Pseudomonas* species and were not further explored in
410 this study that focused on *Pseudomonas* species. Among these, SM412, SM422, SM425,
411 and SM440 showed >95% ANI to *Pseudomonas* sp. NC02, while SM415 and SM430
412 showed >95% to *Pseudomonas* sp. Irchel 3A7 and *Pseudomonas* sp. REP124, respectively.
413 The remaining isolates SM390, SM391, SM393, SM396, SM397, SM404, SM409, and
414 SM431 did not show >95% ANI to any species represented in the GTDB-Tk database,
415 indicating that they may represent previously uncharacterized *Pseudomonas* lineages.

416 We further characterized the isolates using the TYGS, which utilizes a curated database of
417 prokaryotic type strains for whole-genome-based taxonomic classification. This analysis
418 identified isolates belonging to *P. tolaasii, P. pergaminensis, P. agarici, P. simiae, P.*
419 *monsensis,* and *P. yamanorum*, with digital DNA-DNA hybridization (dDDH) values

420 exceeding the 70% species delineation threshold (Meier-Kolthoff et al. 2013), consistent
421 with the results obtained from GTDB-TK classification. In contrast, the *P. tensinigenes*
422 isolate showed a slightly lower dDDH value (66%). However, due to the absence of
423 corresponding valid type strains in the TYGS database, *Pseudomonas "gingeri"*,
424 *Pseudomonas* "*reactans*", and *P. azotoformans* could not be validated. Additionally, the
425 remaining 14 *Pseudomonas* isolates could not be resolved to any known type strain in the
426 database. The complete list of ANI and dDDH values for all isolates is provided in Dataset
427 S01.
428 To assess genetic relatedness among mushroom-associated *Pseudomonas* isolates, we
429 conducted pairwise ANI analyses. Using a ≥95% ANI threshold for species delineation,
430 the dataset resolved into 14 distinct genomic clusters, capturing the full spectrum of intra
431 and interspecific diversity within the collection (Fig. 2A). Comparative analyses with
432 closely related reference type strains enabled the assignment of multiple clusters to
433 recognize species, including *P. "gingeri", P. azotoformans, P. tolaasii, P. pergaminensis,*
434 *P. "reactans", P. agarici, P. simiae, P. monsensis, P. yamanorum*, and *P. tensinigenes*,
435 with clustering patterns aligning with taxonomic classifications derived from TYGS and
436 GTDB analyses. Isolates SM400 and SM426 did not cluster with *P. allokribbensis* and *P.*
437 *azerbaijanoccidens*, respectively, indicating significant genomic divergence from these
438 reference strains. The remaining 14 isolates formed three distinct genomic clusters: Cluster
439 1 (SM412, SM422, SM425, SM440), Cluster 2 (SM391, SM393, SM396), and Cluster 3
440 (SM390, SM397, SM404, SM409, SM431), with SM415 and SM430 representing distinct
441 lineages.
442
443 **3.6. Multi-locus sequence analysis**
444 To evaluate the commonly used MLSA for taxonomic resolution and compare it with
445 phylogenomic inference, we selected eight conserved housekeeping genes *rpoD, rpoB,*
446 *recA, gapA, gltA, atpD, gyrB*, and *ileS* as molecular barcodes based on their established
447 discriminatory power and phylogenetic stability (Gomila et al., 2015). A maximum-
448 likelihood phylogeny was reconstructed from the concatenated sequences of these loci for
449 57 *Pseudomonas* isolates, including 32 type strains.

The largest lineage corresponded to *Pseudomonas* "*gingeri*", comprising 11 isolates. Three major sister clades were resolved, including an independent lineage represented by SM434, while the remaining reference strains formed a separate, well-supported subclade. SM416 grouped with the type strain *P. agarici* LMG 2112^T, forming a distinct and clearly separated lineage. Consistent with ANI and GTDB-Tk assignments, seven isolates clustered with *P. tolaasii* NCPPB 2192^T, while six isolates grouped with *P. pergaminensis* 1008^T and Z7.15^T. Similarly, ten isolates clustered with *P. azotoformans* S4^T, and SM423 and SM450 grouped with *P*. "*reactans*" C5002. Several isolates exhibited broader genomic affinities, with *P. monsensis*, *P. tensinigenes*, *P. allokribbensis,* and *P. azerbaijanoccida* forming closely related yet distinct branches. Furthermore, SM415 and SM430 resolved into two independent lineages. Additional well-supported isolate clusters included SM412, SM422, SM425, SM440; SM391, SM393, SM396; and SM390, SM397, SM404, SM409, and SM431.

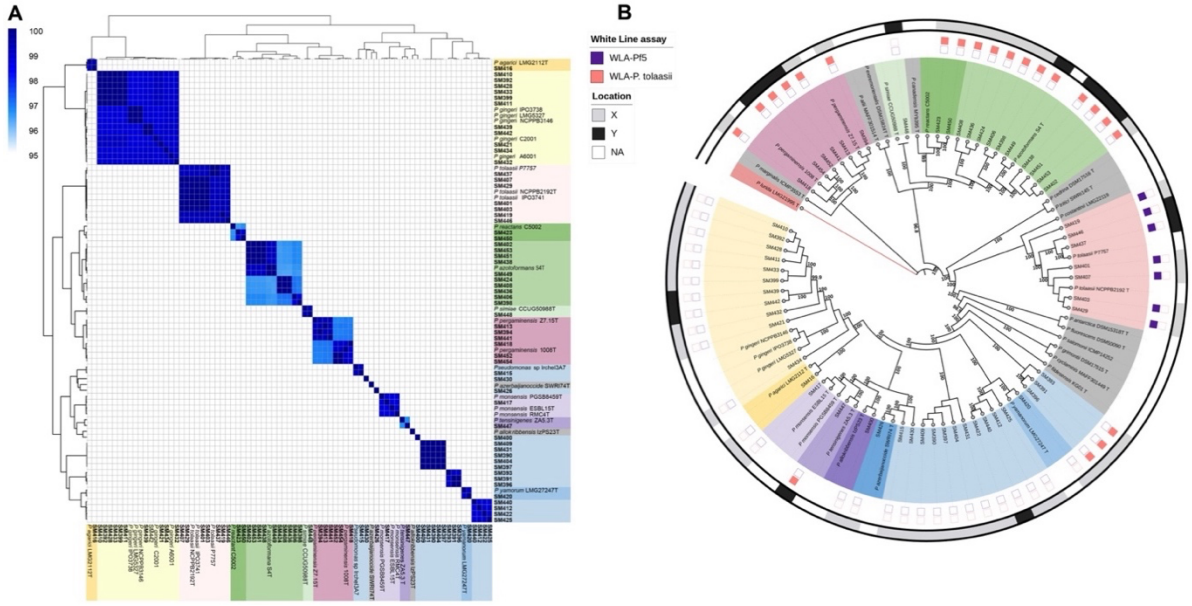

Fig. 2. Genomic taxonomy and phylogenetic relationships of *Pseudomonas* isolates associated with bacterial blotch in white button mushrooms (*Agaricus bisporus*) from two U.S. farms (X and Y). (A) Heatmap of pairwise whole-genome Average Nucleotide Identity (ANI) among 57 blotch-associated isolates and 22 reference strains. Color intensity reflects genome similarity, with values ≥95% indicating species-level identity. Axis labels are color-coded by species cluster. (B) Circular maximum-likelihood phylogenetic tree reconstructed from concatenated sequences of eight housekeeping genes

(*rpoD, rpoB, recA, gapA, gltA, atpD, gyrB, and ileS*) for 57 isolates and 31 reference strains. Bootstrap support values ≥95% are shown; branch lengths are not to scale. *Pseudomonas lurida* served as the outgroup. The outer ring denotes farm origin (X or Y), while inner markers indicate white-line assay results: pink squares = positive interaction with *P. tolaasii* BP1106; purple squares = positive interaction with *P. fluorescens* Pf-5.

3.7. Comparative Pan-Genome Analysis

Roary identified 1,206 core genes and 45,131 accessory genes across the 57 *Pseudomonas* isolates. Among these, 133 soft-core genes were present in at least 95% but fewer than 99% of strains; 9,240 shell genes were present in at least 15% but fewer than 95% of strains; and 35,758 cloud genes were present in at least one strain but fewer than 15%. In total, the pangenome comprised 46,337 genes, highlighting extensive genomic diversity among the isolates. We analyzed the core and pangenome of the four dominant *Pseudomonas* species: *P. tolaasii, P. pergaminensis, P. "gingeri"*, and *P. azotoformans* (Fig. 3). In *P. tolaasii*, the pangenome comprised 8,356 genes, including 5,161 core genes (62%) shared across nearly all isolates, and an accessory genome of 3,195 genes (1,118 shell and 2,077 cloud). *P. pergaminensis* showed a comparable pattern, with a total of 9,092 genes, of which 4,745 (52%) were core; the accessory genome consisted of 2,339 shell and 2,008 cloud genes. *P.* "*gingeri*" harbored 9,026 total genes, including 5,560 core genes (62%) and an accessory component of 1,842 shell and 1,624 cloud genes. These species displayed consistently high core-to-pan-genome ratios, indicating that most isolates share a conserved set of essential metabolic and structural functions.

In contrast, *P. azotoformans* exhibited a markedly expansive pan-genome, with 18,029 genes but only 2,477 core genes (14%). Its accessory genome was dominated by 6,858 shell and 8,694 cloud genes, reflecting extensive genomic variability and a substantially more flexible gene repertoire.

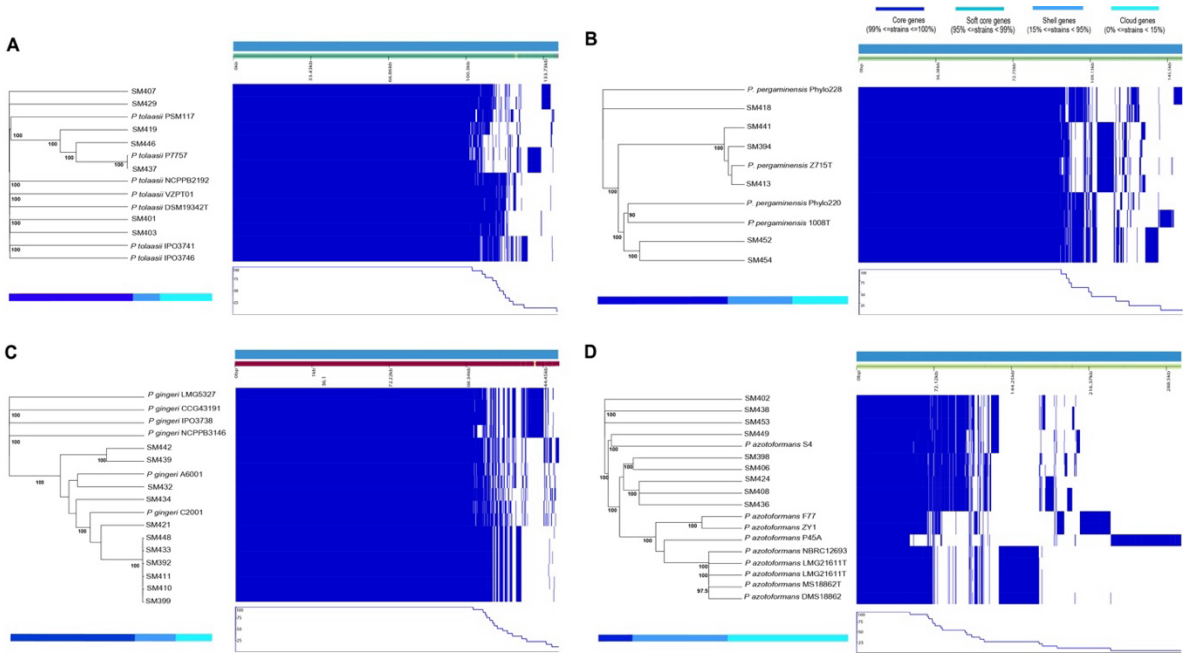

Fig. 3. Core and pangenome architecture of four *Pseudomonas* species associated with bacterial blotch in white button mushrooms (*Agaricus bisporus*) from two U.S. farms (X and Y). (A) *P. tolaasii;* (B) *P. pergaminensis;* (C) *Pseudomonas "gingeri";* (D) *P. azotoformans.* Each panel shows a maximum-likelihood phylogenetic tree based on core gene alignments for the respective species cluster, alongside a gene presence–absence matrix. Rows correspond to individual genomes; columns represent orthologous gene families. Blue blocks indicate gene presence; white blocks indicate absence. Bar graphs summarize the proportion of core, soft-core, shell, and cloud genes, illustrating species-specific genomic diversity and accessory genome expansion.

3.8. Diversity and distribution of biosynthetic gene clusters among *Pseudomonas* isolates

Beyond DNA-based taxonomy, we generated *in silico* secondary metabolite profiles to examine chemotaxonomic patterns among blotch-associated *Pseudomonas* species. Genome mining of the 57 *Pseudomonas* isolates using antiSMASH revealed a substantial biosynthetic diversity, encompassing 22 distinct families of secondary metabolite biosynthetic gene clusters (BGC) (Fig. 4). The presence-absence matrix illustrates the distribution of major BGC classes, including numerous nonribosomal peptide synthetase (NRPS) loci encoding cyclic lipopeptides such as tolaasin, viscosin, ririwpeptide, lokisin, syringafactin, putisolvin, orfamides B, syringocin, histicorrugatin, necroxime, stechlisin,

sessilin, bananamide, and corpeptin-like families. Siderophore-associated clusters were abundant and phylogenetically widespread, including EDHA, yersiniabactin, Ni-siderophore, enantio-pyochelin, and azotobactin D. Several isolates also encoded BGCs for volatile or antibiotic metabolites such as sodorifen, geosmin, and 2,4-diacetylphloroglucinol. Distinct chemotaxonomic signatures emerged across species: *P. gingeri* encoded volatile and antibiotic loci; *P. pergaminensis* consistently carried viscosin; *P. tolaasii* harbored tolaasin; and viscosin clusters were widely distributed across several lineages, including *P. "reactans"*. Cluster-specific patterns were evident, with Cluster 1 enriched in enantio-pyochelin and Cluster 3 encoding combinations of tolaasin and riripeptide like loci. Notably, *P. azotoformans* lacked known BGCs for CLPs, siderophores, volatiles, or antibiotics, suggesting unexplored or cryptic metabolic pathways.

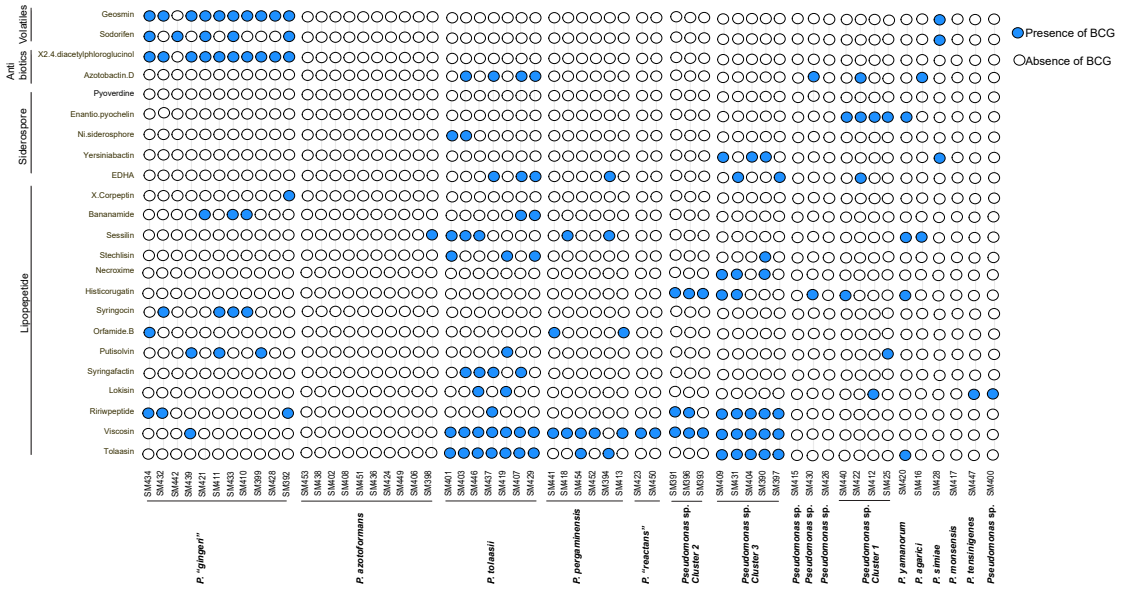

Fig. 4. Distribution of 22 Biosynthetic gene cluster (BGC) families across 57 *Pseudomonas* isolates. Columns represent individual isolates, and rows correspond to BGCs families grouped into four functional categories: lipopeptides, siderophores, antibiotics, and volatiles. Blue dots indicate predicted presence of a BGC family with ≥30% sequence similarity as predicted by antiSMASH, while white dots indicate absence. Presence may include both complete and partial clusters, as predicted by antiSMASH.

571 **3.9. Pathogenicity assessment**

572 To assess the range of symptom patterns we monitored disease progression over a 48-hour
573 period after inoculation. In Fig. 5 we summarized the symptoms induced by individual
574 *Pseudomonas* species on mushroom cap tissues. Apart from the characteristic "brown
575 blotch" and "ginger blotch" symptoms caused by *P. tolaasii* and *Pseudomonas* "gingeri,"
576 respectively, the additional species identified in this study produced distinct lesion
577 phenotypes. For instance, *P. pergaminensis* induced lighter brown lesions accompanied by
578 pronounced tissue pitting, whereas *P. yamanorum* generated pale yellow discoloration,
579 also associated with noticeable pitting. In contrast, isolates belonging to Cluster 3 were
580 mainly associated with dark, chocolate-brown discoloration and fine, needle-like pitting as
581 the infection progressed. Isolates from Cluster 1 produced pale brown lesions with limited
582 pitting but evident tissue damage. *P. azotoformans* caused irregular brown blotches with
583 slight pitting progression, while *P. agarici* produced wet, yellowish tissue with little or no
584 pitting. *P. monsensis* and *P. tensinigenes* both exhibited dark black discoloration without
585 significant tissue damage or pitting. Furthermore, *P. simiae,* isolates in Cluster 2, SM400,
586 and SM426 caused only slight discoloration compared to the nonpathogenic control.

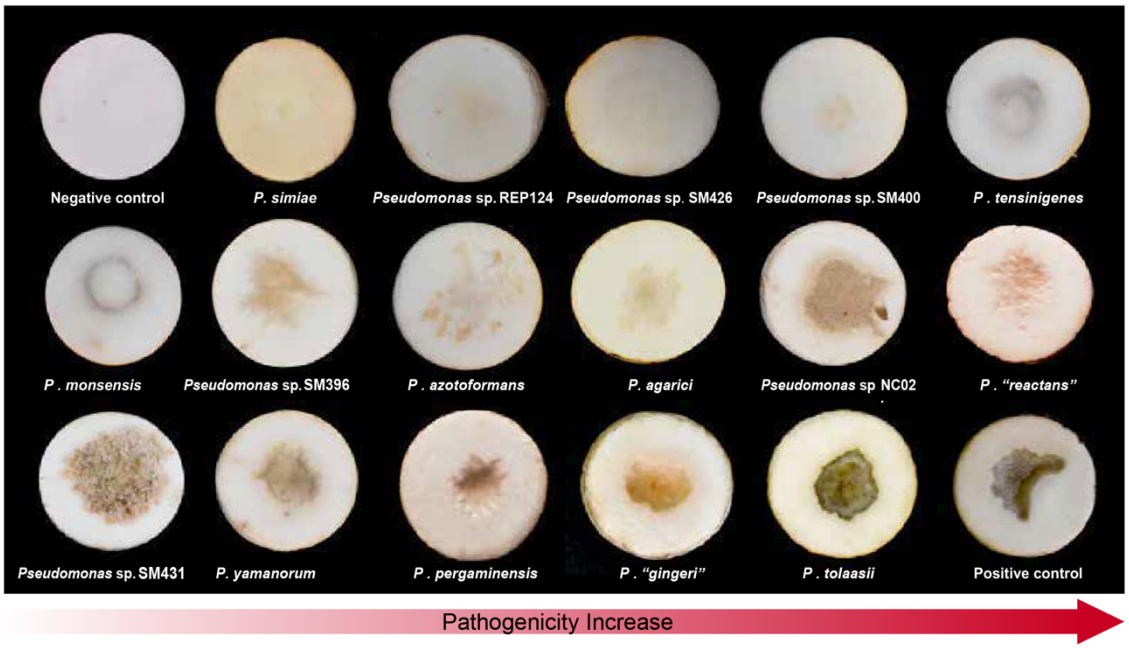

587 **Fig. 5. Pathogenicity assays of representative *Pseudomonas* species clusters inoculated**
588 **on fresh white button mushroom tissue**. Lesion phenotypes range from extensive

589 discoloration with pronounced tissue pitting to rapid surface browning and mild or slow
590 discoloration. Arrows indicate increasing pathogenic severity across species clusters.
591
592 **4. DISCUSSION**
593
594 In this study, we isolated and characterized bacterial blotch-causing *Pseudomonas* from
595 white button mushrooms collected from two southern states in the USA. Among the 56
596 isolates, we identified well-known blotch pathogens, including *Pseudomonas "gingeri*"
597 (*n* = 11), *P. tolaasii* (*n* = 7), *Pseudomonas* sp. NC02 (*n* = 4), and *Pseudomonas "reactans"*
598 (*n* = 2), along with single isolates of *P. yamanorum*, and *P. agarici*. Additionally, we
599 identified seven bacterial taxa that had not been previously reported as associated with
600 blotch disease, including *P. azotoformans* (*n* = 10), *P. pergaminensis* (*n* = 6), *P. monsensis*,
601 *P. tensinigenes*, *P. simiae*, *Pseudomonas* sp. Irchel 3A7, and *Pseudomonas* sp. REP124A.
602 Furthermore, we identified two distinct lineages of previously unrecognized *Pseudomonas*
603 spp., representing putative novel species associated with blotch symptoms. The strains
604 SM391, SM393, and SM396 formed one group, while the strains SM390, SM397, SM404,
605 SM409, and SM431 formed another, each constituting well-supported, genomically
606 coherent clades according to ANI, dDDH and MLSA.
607 Accurate species identification is essential for understanding pathogen diversity and
608 informing disease management strategies. To resolve the taxonomy of the *Pseudomonas*
609 isolates recovered in this study, we applied multiple complementary approaches, including
610 TYGS, GTDB-TK, ANI, and MLSA. Together, these methods provided a robust
611 framework for evaluating genomic relatedness and enabled high-confidence species
612 assignments. Using this integrative strategy, we clearly resolved several blotch-associated
613 taxa, including *Pseudomonas* "gingeri", *P. tolaasii*, *P.* "*reactans*", *P. yamanorum*, *P.*
614 *agarici*, *P. azotoformans*, *P. pergaminensis*, *P. monsensis*, and *P. simiae*, effectively
615 distinguishing our isolates from their closest type strains. However, some groups required
616 more nuanced interpretation. For example, MLSA clustered isolates SM400 and SM426
617 near *P. allokribbensis* IzPS23^{T} and *P. azerbaijanoccidentalis* SWRI74^{T}, yet ANI and
618 GTDB-TK-based dDDH values demonstrated clear genomic distinctiveness, supporting
619 their classification as independent species. Likewise, isolate SM447 showed <70% dDDH
620 similarity to *P. tensinigenes* based on TYGS; however, ANI-based inference provided

621 improved resolution at the species level. A subset of four isolates (SM412, SM422, SM425,
622 SM440) was identified as *Pseudomonas* sp. NC02 according to GTDB-TK. Due to
623 insufficient genome quality for these reference taxa, they could not be fully evaluated using
624 FastANI or MLSA methods. Therefore, we applied GGDC, which confirmed that all four
625 isolates belong to the *Pseudomonas* sp. NC02 lineage. Similarly, SM430 and SM415
626 identified to be *Pseudomonas* sp. REP124 and *Pseudomonas* sp. Irchel 3A7, respectively.
627 Together, these results highlighted the necessity of multi-method taxonomic frameworks
628 when describing *Pseudomonas* diversity in the mushroom environment. Further, we
629 highlight the inherent differences in resolution between marker gene-based and whole-
630 genome approaches. MLSA, while useful for initial phylogenetic placement and continuity
631 with historical taxonomy, may lack sufficient discriminatory power for closely related taxa
632 due to its reliance on a limited number of conserved loci (Gomila et al., 2015). In contrast,
633 ANI and digital dDDH, which incorporate genome-wide information, provide more robust
634 and reproducible criteria for species delineation. Therefore, in cases of conflict, genome-
635 based approaches should be prioritized, with ANI (≥95%) and dDDH (≥70%) serving as
636 primary criteria for species delineation, while MLSA should be used as a complementary
637 tool to provide phylogenetic context rather than define taxonomic boundaries. BOX-PCR
638 fingerprinting proved valuable as an initial screening tool to capture genomic diversity
639 across all 76 blotch-associated isolates. Although BOX-PCR revealed substantial
640 heterogeneity, its clustering patterns did not correspond with ANI or MLSA-based
641 phylogenies, reflecting differences in repetitive element dynamics rather than true
642 evolutionary relationships. As seen in other bacterial genera such as *Streptomyces*, BOX-
643 PCR is well-suited for rapid delineation of non-redundant isolates but offers limited
644 resolution for deeper taxonomic or phylogenetic inference (Nayak et al., 2011; Rademaker
645 et al., 1998; Van Belkum et al.,1996). Accordingly, in this study, it served primarily as a
646 high-throughput preselection method prior to whole-genome analyses.
647 Among the novel blotch-associated taxa identified in this study, *Pseudomonas*
648 *azotoformans* was particularly abundant, representing a notable expansion of the known
649 ecological range of this species. *P. azotoformans* has primarily described in plant-
650 associated contexts, most notably as a pathogen of cereal crops such as rice (Iizuka and

651 Komagata 1963), and as an antagonist of several important plant pathogens, including
652 *Fusarium fujikuroi* (Wiemann et al., 2013), *Colletotrichum* spp. (Popescu et al., 2024),
653 *Pseudomonas syringae* pv. *actinidiae* (Correia et al., 2025), and *Alternaria brassicae*
654 (Bhattacharya et al., 2025). This host expansion may be facilitated by the species
655 exceptional tolerance to a wide range of abiotic stresses, including heavy metals, salinity,
656 drought, antibiotics, and extreme temperatures, traits that likely enhance persistence in
657 managed agricultural environments. In support of its ecological versatility, *P.*
658 *azotoformans* has also been implicated in the blue discoloration of rabbit carcasses
659 (Circella et al., 2022) and detected in food-processing environments (Thomassen et al.,
660 2022). Overall, *P azotoformans* appears to be a highly adaptable generalist, capable of
661 colonizing diverse hosts and ecological niches. Its prevalence in mushroom blotch may be
662 facilitated by its ability to persist in acidic substrates (Mokrani et al., 2020; Wang et al.,
663 2021), such as peat moss, a primary component of mushroom casing soil. However, their
664 prevalence in bacterial blotch disease highlights the need of future studies on its
665 evolutionary trajectory, host range, transmission pathways, and virulence mechanisms to
666 understand its role in emerging disease complexes across agricultural and food systems. In
667 addition to *P. azotoformans*, we also reported the first association of *P. pergaminensis* with
668 mushroom blotch. This species was originally isolated from the wheat rhizosphere during
669 tillering (Díaz et al., 2022) and is used as a bio-stimulant to enhance crop performance.
670 While not previously linked to mushroom pathogenesis, *P. pergaminensis* possesses
671 genomic traits consistent with rhizosphere competence, including phosphate and zinc
672 solubilization and the secretion of extracellular lytic enzymes such as phospholipases and
673 proteases (Díaz et al., 2022; Xiang et al., 2025) which may similarly facilitate colonization
674 and symptom development on mushroom tissues.
675 The mechanisms underlying discoloration and pitting caused by *Pseudomonas* species
676 remain poorly understood. However, accumulating evidence suggests that extracellular
677 metabolites, such as cyclic lipopeptides (tolaasin), siderophores, degradative enzymes
678 (proteases and lipases), and volatiles (tovsins, DMDS), play central roles in tissue
679 degradation and corrosion processes (Lo Cantore et al., 2015; Soler-Rivas et al., 1999).
680 These compounds mediate microbial competition, surface colonization, and host-pathogen

681 interactions, all of which may contribute to blotch-like symptoms on mushroom caps. To
682 explore this biochemical basis, we employed antiSMASH to predict the families of
683 secondary metabolites encoded by all isolates and to assess their diversity and distribution.
684 Heterogeneity in BGCs was evident across isolates, encompassing CLPs, siderophores,
685 antibiotics, and volatile compounds. CLPs represent a major class of multifunctional
686 secondary metabolites predominantly produced by *Pseudomonas* spp. Among the CLPs,
687 WLIP has been identified as a diagnostic marker for the interaction between tolaasin and
688 the cyclic WLIP produced by *Pseudomonas "reactans"* (Rokni-Zadeh et al., 2011), which
689 manifests as a dense white line when the two strains are grown adjacently on agar. The
690 white line reaction is highly structure-specific; WLIP analogues such as viscosin,
691 containing L-Leu instead of D-Leu at position 5, and viscosinamide, a viscosin variant with
692 D-Gln replacing D-Glu at position 2, fail to induce a white line in the presence of *P. tolaasii*
693 (Rokni-Zadeh et al., 2011; Rokni-Zadeh et al., 2013), highlighting the strict molecular
694 complementarity between WLIP and tolaasin. However, accumulating evidence indicates
695 that this interaction is not exclusive. CLPs other than WLIP, including orfamides A,
696 viscosin, and massetolide A, can also form visible white lines with tolaasin (Henkels et al.
697 2014). Similarly, sessilins, which are structurally related to tolaasin, induce white line
698 formation through co-precipitation with orfamides (D'aes et al., 2014). Further evidence
699 suggests that WLIP secretion is not restricted to *P. reactans*; *P. fluorescens* and *P. putida*
700 strains also produce WLIP (Rokni-Zadeh et al., 2012). In the present study, we observed
701 similar results related to WLIP. *Pseudomonas pergaminensis*, which produces viscosin and
702 orfamides B but no detectable WLIP, formed a clear white line with *P. tolaasii* BP1106.
703 *P. azotoformans*, despite limited CLP production, also induced a white line. Notably, *P.*
704 *aeruginosa* LMG 1272, which lacks canonical CLP biosynthetic genes associated with
705 WLR, nonetheless forms a precipitate when co-cultured with *P. tolaasii* (Salari et al.,
706 2020). Additionally, *Pseudomonas* species cluster 2 isolates (SM391, SM393, and
707 SM396), which are positive for viscosin production, produced detectable white lines when
708 confronted with *P. tolaasii* BP1106. These observations suggest that WLR formation is not
709 strictly dependent on a single WLIP-tolaasin pair. Rather, variations in peptide
710 stereochemistry, fatty acid chain length, or CLP production levels may influence diffusion

711 and co-precipitation dynamics, resulting in differences in white line intensity and
712 morphology. Siderophore BGCs, including EDHA, yersiniabactin, Ni-siderophore,
713 enantio-pyochelin, and azotobactin D, were distributed among the isolates, consistent with
714 the central role of iron acquisition in bacterial fitness (Page, 2013; Jimenez et al., 2010).
715 However, the canonical siderophore pyoverdine, commonly associated with fluorescent
716 *Pseudomonas* species, was not detected at sufficient similarity levels in any of the
717 genomes. Furthermore, although tolaasin-like clusters were detected with moderate
718 similarity (50–75%) in *P. pergaminensis*, *P. yamanorum*, and species cluster 3, white-line
719 agar assays confirmed the absence of tolaasin activity. Taken together, these results
720 highlight both the utility and the limitations of *in silico* BGC predictions: while they
721 provide valuable chemotaxonomic signatures and candidate loci of interest, functional
722 validation including domain-level annotation, proteomics, metabolomic analyses is
723 necessary to confirm metabolite production and their direct contributions to virulence.
724 Comparative pangenome analysis of *Pseudomonas tolaasii*, *P. pergaminensis*, *P.* "*gingeri*"
725 and *P. azotoformans* revealed that only *P. azotoformans* possessed a significantly larger
726 accessory genome relative to its core genome. This expanded accessory fraction
727 corresponds with its broad ecological distribution, siderophore production, and
728 environmental tolerance, reflecting high genomic plasticity for rapid adaptation. To assess
729 the genetic diversity and expansion potential of the four *Pseudomonas* species, we analyzed
730 their pan-genome trajectories using Tettelin et al.'s (2008) power-law regression model,
731 based on Heaps' Law. In this framework, the number of new genes discovered with each
732 additional genome sequenced is described mathematically by $Yp = Ax^{\wedge}B + C$, where γ
733 (exponent B) indicates pan-genome openness: $\gamma > 0$ denotes an open pan-genome, with
734 genes continuing to accumulate, while $\gamma < 0$ denotes a closed pan-genome, where new gene
735 discovery slows substantially. The Estimated γ values were 0.049 (*P. tolaasii*), 0.056 (*P.*
736 *pergaminensis*), 0.046 (*P. "gingeri"*), and 0.085 (*P. azotoformans*). According to the
737 power-law framework results indicate that all species possess theoretically open
738 pangenomes, consistent with continued gene acquisition as additional genomes are
739 incorporated. However, the relatively low γ values suggest that these pangenomes may be
740 nearing closure. These interpretations should be approached with caution, as limited

741 genome sampling can affect the reliability of power-law extrapolation. Consistent with our
742 findings, previous studies have also reported an open pangenome for *Pseudomonas tolaasii*
743 (Liu et al., 2022), although comprehensive comparative data across related species remain
744 limited.
745 While the study is limited by a narrow temporal window and sampling restricted to two
746 southern U.S. farms, future research will incorporate comparative analyses of both
747 symptomatic and asymptomatic mushrooms, following the approach of Martins et al.
748 (2020), to establish baseline microbiome diversity. The findings presented here enhance
749 the current understanding of blotch disease etiology, revealing a greater taxonomic and
750 functional diversity among the pathogens than previously recognized, and extending global
751 insights into the complex bacterial community responsible for mushroom blotch. To our
752 knowledge, this study provides the first evidence that *P. azotoformans*, *P. pergaminensis*,
753 *P. monsensis*, *P. tensinigenes*, and *P. simiae* cause blotch in *Agaricus bisporus*, overturning
754 the long-held assumption that the disease is primarily driven by *P. tolaasii* and *P.*
755 *"gingeri"*. Species identities were robustly resolved through ANI, TYGS, GTDB-TK and
756 GGDC. Secondary metabolite profiling and white-line assays further uncovered molecular
757 features likely contributing to virulence and competitive fitness. The substantial diversity
758 among pathogens, with *P. azotoformans* showing pronounced genomic expansion
759 indicative of broad ecological adaptability. As newly emerging pathogens become
760 increasingly prevalent, strain-level diagnostics and genomic surveillance will be critical
761 for early detection and improved disease management in commercial mushroom
762 production.
763

764 **5. CREDIT AUTHORSHIP CONTRIBUTION STATEMENT**

765 **Author Contributions:** S.J.M. obtained the funding source; S.D.M., S.J.M., and R.G.
766 designed the research; S.D.M. performed experiments; S.J.M. and M.L. assisted with
767 experimental work; J.H. contributed to bioinformatics analyses; S.D.M. wrote the
768 manuscript; R.G., and S.J.M reviewed the manuscript.
769
770

6. DECLARATION OF COMPETING INTEREST:

The authors declare no competing interests.

7. ACKNOWLEDGMENTS

The authors also acknowledge Dr. Fabiano Perina for the assistance with the rep-PCR assay and Dr. Carolee Bull who kindly shared the bacterial strains BP1304, BP1106 and *P. florescens* Pf-5 used in this study.

8. STUDY FUNDING

This work was supported by the USDA SCRI: PENW-2023-05649 and by the Research Capacity Fund (Hatch) program, project award no. 7010682, from the U.S. Department of Agriculture's National Institute of Food and Agriculture.

9. DATA AVAILABILITY

The whole genome data generated during the current study are available in the NCBI under Bio Project PRJNA1377199, with accession numbers SAMN53759319 to SAMN53759375.

10. REFERENCES

1. Atila, F., Nadhim Owaid, M., & Ali Shariati, M. (2017). The nutritional and medical benefits of *Agaricus bisporus* : a review. J. Microbiol. Biotechnol. Food Sci. *7*(3), 281–286. https://doi.org/10.15414/jmbfs.2017/18.7.3.281-286
2. Bankevich, A., Nurk, S., Antipov, D., et al., 2012. SPAdes genome assembly algorithm and its applications to single-cell sequencing. J Comput Biol. 19, 455–477. http://doi.org/10.1089/cmb.2012.0021
3. Bhattacharya, A., Verma, P., Bharti, C., et al., 2025. Characterization of antifungal metabolites of *Pseudomonas azotoformans* SS7 from *Brassica juncea* as a biocontrol tool for *Alternaria brassicae*. Arch. Phytopathol. Plant Prot. 58, 604–629. https://doi.org/10.1080/03235408.2024.2415157
4. Blin, K., Shaw, S., Augustijn, H.E., et al., 2023. antiSMASH 7.0: new and improved predictions for detection, regulation, chemical structures and visualization. Nucleic Acids Res. 51, W46–W50. https://doi.org/10.1093/nar/gkad344
5. Chaumeil, P.A., Mussig, A.J., Hugenholtz, P., et al., 2022. GTDB-Tk v2: Classification with the genome taxonomy database. Bioinformatics. 38, 5315–5316. https://doi.org/10.1093/bioinformatics/btac672

806 6. Chen, S., Zhou, Y., Chen, Y., et al., 2018. fastp: an ultra-fast FASTQ preprocessor.
807 Bioinformatics. 34, i884–i890. https://doi.org/10.1093/bioinformatics/bty560
808 7. Circella, E., Casalino, G., Camarda, A., et al., 2022. *Pseudomonas fluorescens* group
809 bacteria causing chromatic alteration of rabbit carcasses. Ital. J. Food Saf. 11, 10042.
810 https://doi.org/10.4081/ijfs.2022.9998
811 8. Correia, C., Cellini, A., Donati, I., et al., 2025. *Pseudomonas azotoformans* and
812 *Pseudomonas putida*: novel kiwifruit-native biological control agents against
813 *Pseudomonas syringae* pv. *actinidiae*. Biol. Control. 201, 105706.
814 https://doi.org/10.1016/j.biocontrol.2025.105706
815 9. D'aes, J., Kieu, N.P., Léclère, V., et al., 2014. To settle or to move? Interplay between
816 cyclic lipopeptides in *Pseudomonas* CMR12a. Environ. Microbiol. 16, 2282–2300.
817 http://doi.org/10.1111/1462-2920.12462
818 10. Díaz, M., Bach, T., González Anta, G., et al., 2022. Agronomic efficiency and genome
819 mining analysis of the wheat-biostimulant rhizospheric bacterium *Pseudomonas*
820 *pergaminensis* sp. nov. strain 1008T. Front. Plant Sci. 13, 894985.
821 https://doi.org/10.3389/fpls.2022.894985
822 11. Eger, G., 1972. Experiments and comments on the action of bacteria on sporophore
823 initiation in *Agaricus bisporus*. Mushroom Sci. 8, 719–725.
824 12. Fatmi, M., Collmer, A., Iacobellis, N.S., et al., 2008. *Pseudomonas syringae* pathovars
825 and related pathogens: identification, epidemiology and genomics. Springer,
826 Dordrecht. https://doi.org/10.1007/978-1-4020-6901-7
827 13. Fermor, T., Lincoln, S., Noble, R., et al., 2000. Microbiological properties of casing.
828 Mushroom Sci. 15, 447–454.
829 14. Geels, F.P., Hesen, L.P.W., van Griensven, L.J.L.D.M., 1994. Brown discolouration of
830 mushrooms caused by *Pseudomonas agarici*. J. Phytopathol. 140, 249–259.
831 https://doi.org/10.1111/j.1439-0434.1994.tb04814.x
832 15. Godfrey, S.A.C., Marshall, J.W., Klena, J.D., 2001. Genetic characterization of
833 *Pseudomonas* 'NZI7', a novel pathogen causing brown blotch disease of *Agaricus*
834 *bisporus*. J. Appl. Microbiol. 91, 412–420. https://doi.org/10.1046/j.1365-
835 2672.2001.01398.x
836 16. Gomila, M., Peña, A., Mulet, M., et al., 2015. Phylogenomics and systematics in
837 *Pseudomonas*. Front. Microbiol. 6, 214. https://doi.org/10.3389/fmicb.2015.00214
838 17. Gurevich, A., Saveliev, V., Vyahhi, N., et al., 2013. QUAST: quality assessment of
839 genome assemblies. Bioinformatics. 29, 1072–1075.
840 http://doi.org/10.1093/bioinformatics/btt086
841 18. Hadfield, J., Croucher, N.J., Goater, R.J., et al., 2018. Phandango: an interactive viewer
842 for bacterial population genomics. Bioinformatics. 34, 292–293.
843 https://doi.org/10.1093/bioinformatics/btx610
844 19. Hamidizade, M., Taghavi, S.M., Martins, S.J., et al., 2020. Bacterial brown pit, a new
845 disease of edible mushrooms caused by *Mycetocola* sp. Plant Dis. 104, 1445–1454.
846 https://doi.org/10.1094/PDIS-10-19-2176-RE
847 20. Henkels, M.D., Kidarsa, T.A., Shaffer, B.T., et al., 2014. *Pseudomonas protegens* Pf-
848 5 causes discoloration and pitting of mushroom caps due to antifungal metabolites.
849 Mol. Plant-Microbe Interact. 27, 733–746. https://doi.org/10.1094/MPMI-10-13-0311-
850 R

21. Huang, Z., Huang, Y., Nie, Y., et al., 2024. Biological characteristics of two pathogens causing brown blotch in *Agaricus bisporus* and toxin identification of *Cedecea neteri*. Phytopathol. Res. 6, 21. https://doi.org/10.1186/s42483-024-00239-8
22. Huang, Z., Li, F., Li, H., et al., 2026. First report of *Pseudomonas extremorientalis* causing brown blotch disease of white button mushroom (*Agaricus bisporus*) in China. Plant Dis. 110, 214. https://doi.org/10.1094/PDIS-06-25-1178-PDN
23. Iizuka, H., Komagata, K., 1963. New species of *Pseudomonas* belonging to the fluorescent group. Bull. Agric. Chem. Soc. Jpn. 37, 137–141. https://api.semanticscholar.org/CorpusID:88112541
24. Jaccard, P., 1908. Nouvelles recherches sur la distribution florale. Bull. Soc. Vaud. Sci. Nat. 44, 223–270.
25. Jain, C., Rodriguez-R, L.M., Phillippy, A.M., et al., 2018. High-throughput ANI analysis reveals clear species boundaries. Nat. Commun. 9, 5114. https://doi.org/10.1038/s41467-018-07641-9
26. Jimenez, P.N., Koch, G., Papaioannou, E., et al., 2010. Role of PvdQ in *Pseudomonas aeruginosa* virulence under iron-limiting conditions. Microbiology. 156, 49–59. http://doi.org/10.1099/mic.0.030973-0
27. King, E.O., Ward, M.K., Raney, D.E., 1954. Two simple media for demonstration of pyocyanin and fluorescin. J. Lab. Clin. Med. 44, 301–307. https://pubmed.ncbi.nlm.nih.gov/13184240
28. Letunic, I., Bork, P., 2024. Interactive Tree of Life (iTOL) v6: recent updates to the phylogenetic tree display and annotation tool. Nucleic Acids Res. 52, W78–W82. https://doi.org/10.1093/nar/gkae268
29. Li, Z., Zhang, M., Liu, Y., et al., 2025. Advances in the preparation, structure-activity relationship, and biological mechanisms of *Agaricus* polysaccharides. Food Sci. Hum. Wellness. https://doi.org/10.26599/FSHW.2025.9250590
30. Liu, Z., Zhao, Y., Sossah, L.F., et al., 2022. Characterization, pathogenicity, phylogeny, and comparative genomic analysis of *Pseudomonas tolaasii* strains isolated from various mushrooms in China. Phytopathology. 112, 521–534. https://doi.org/10.1094/PHYTO-12-20-0550-R
31. Lo Cantore, P., Giorgio, A., Iacobellis, N.S., 2015. Bioactivity of volatile organic compounds produced by *Pseudomonas tolaasii*. Front. Microbiol. 6, 1082. https://doi.org/10.3389/fmicb.2015.01082
32. Martins, S.J., Trexler, R.V., Vieira, F.R., Pecchia, J., Kandel, P., Hockett, K., Bell, T.H., Bull, C.T., 2020. Comparing approaches for capturing bacterial assemblages associated with symptomatic (bacterial blotch) and asymptomatic mushroom (*Agaricus bisporus*) caps. Phytobiomes J. 4, 90-99, https://doi:10.1094/PBIOMES-08-19-0044-R
33. Meier-Kolthoff, J.P., Auch, A.F., Klenk, H.P., Göker, M., 2013. Genome sequence-based species delimitation with confidence intervals and improved distance functions. BMC Bioinform. 14, 60. http://doi.org/10.1186/1471-2105-14-60
34. Meier-Kolthoff, J.P., Carbasse, J.S., Peinado-Olarte, R.L., et al., 2022. TYGS and LPSN database tandem for fast and reliable genome-based classification and nomenclature of prokaryotes. Nucleic Acids Res. 50, D801–D807. http://doi.org/10.1093/nar/gkab902

895 35. Meier-Kolthoff, J.P., Göker, M., 2019. TYGS: automated genome-based taxonomy.
896 Nat. Commun. 10, 2182. https://doi.org/10.1038/s41467-019-10210-3
897 36. Minh, B.Q., Schmidt, H.A., Chernomor, O., et al., 2020. IQ-TREE 2: new models and
898 efficient methods for phylogenetic inference in the genomic era. Mol. Biol. Evol. 37,
899 1530–1534. https://doi.org/10.1093/molbev/msaa015
900 37. Mokrani, S., Nabti, E.H., 2020. Heavy metal resistance and bioremediation capacity of
901 rhizospheric strain BioRPaz-3 *Pseudomonas azotoformans* endowed with antifungal
902 activities and multi-abiotic stress tolerance in vitro. SN Appl. Sci. 2, 1985.
903 https://doi.org/10.1007/s42452-020-03828-2
904 38. Morihara, K., Homma, J.Y., 1985. Bacterial enzymes and virulence, in: Holder, I.A.
905 (Ed.), Bacterial Enzymes and Virulence. CRC Press, Boca Raton, FL, pp. 41–79.
906 39. Munsch, P., Geoffroy, V.A., Alatossava, T., et al., 2000. Application of siderotyping
907 for characterization of *Pseudomonas tolaasii* and "*Pseudomonas reactans*". Appl.
908 Environ. Microbiol. 66, 4834–4841. https://doi.org/10.1128/AEM.66.11.4834-
909 4841.2000
910 40. Nayak, B.S., Badgley, B., Harwood, V.J., 2011. Comparison of genotypic and
911 phylogenetic relationships of environmental *Enterococcus* isolates by BOX-PCR
912 typing and 16S rRNA gene sequencing. Appl. Environ. Microbiol. 77, 5050–5055.
913 https://doi.org/10.1128/AEM.00130-11
914 41. Osdaghi, E., Martins, S.J., Ramos-Sepulveda, L., et al., 2019. 100 years since Tolaas:
915 bacterial blotch of mushrooms in the 21st century. Plant Dis. 103, 2714–2725.
916 https://doi.org/10.1094/PDIS-03-19-0589-FE
917 42. Page, A.J., Cummins, C.A., Hunt, M., et al., 2015. Roary: large-scale prokaryote pan-
918 genome analysis. Bioinformatics. 31, 3691–3693.
919 https://doi.org/10.1093/bioinformatics/btv421
920 43. Page, M.G.P., 2013. Siderophore conjugates. Ann. N. Y. Acad. Sci. 1277, 115–126.
921 https://doi.org/10.1111/nyas.12024
922 44. Parte, A.C., Sardà Carbasse, J., Meier-Kolthoff, J.P., et al., 2020. List of Prokaryotic
923 names with Standing in Nomenclature (LPSN) moves to the DSMZ. Int. J. Syst. Evol.
924 Microbiol. 70, 5607–5612. http://doi.org/10.1099/ijsem.0.004332
925 45. Popescu, I., Loganathan, A.K., Graham, H.R., et al., 2024. Antifungal activity of
926 *Bacillus velezensis* and *Pseudomonas azotoformans* isolated from compost tea against
927 anthracnose (*Colletotrichum* spp.) on strawberry fruit. Plant Pathol. 73, 2419–2428.
928 https://doi.org/10.1111/ppa.13983
929 46. Rademaker, J.L.W., Louws, F.J., de Bruijn, F.J., 1998. Characterization of microbial
930 diversity by rep-PCR genomic fingerprinting, in: Van Elsas, J.D., et al. (Eds.),
931 Molecular Microbial Ecology Manual. Kluwer Academic, Dordrecht.
932 47. Rokni-Zadeh, H., Li, W., Sanchez-Rodriguez, A., et al., 2012. Genetic and functional
933 characterization of cyclic lipopeptide white-line-inducing principle (WLIP) production
934 by rice rhizosphere isolate *Pseudomonas putida* RW10S2. Appl. Environ. Microbiol.
935 78, 4826–4834. http://doi.org/10.1128/AEM.00335-12
936 48. Rokni-Zadeh, H., Li, W., Yilma, E., et al., 2013. Distinct lipopeptide systems for WLIP
937 (white line-inducing principle) in *Pseudomonas fluorescens* and *Pseudomonas putida*.
938 Environ. Microbiol. Rep. 5, 160–169. http://doi.org/10.1111/1758-2229.12015

939 49. Rokni-Zadeh, H., Mangas-Losada, A., De Mot, R., 2011. PCR detection of NRPS
940 genes in lipopeptide-producing *Pseudomonas*. Microb. Ecol. 62, 941–947.
941 http://doi.org/10.1007/s00248-011-9885-9
942 50. Royse, D.J., Baars, J., Tan, Q., 2017. Current overview of mushroom production in the
943 world, in: Zied, D.C., Pardo-Giménez, A. (Eds.), Edible and Medicinal Mushrooms:
944 Technology and Applications. Wiley-Blackwell, Hoboken, NJ, pp. 5–13.
945 51. Saha, R., Saha, N., Donofrio, R.S., et al., 2013. Microbial siderophores: a mini-review.
946 J. Basic Microbiol. 53, 303–317. http://doi.org/10.1002/jobm.201100552
947 52. Salari, F., Zare-Mirakabad, F., Alavi, M.H., Girard, L., et al., 2020. Draft genome
948 sequence of *Pseudomonas aeruginosa* LMG 1272, an atypical white line reaction
949 producer. Microbiol. Resour. Announc. 9, e01363-19.
950 https://doi.org/10.1128/mra.01363-19
951 53. Sánchez-Jaramillo, E.A., Gasca-Lozano, L.E., Vera-Cruz, J.M., et al., 2022.
952 Automated image analysis for kidney fibrosis. Biology (Basel). 11, 1227.
953 http://doi.org/10.3390/biology11081227
954 54. Seemann, T., 2014. Prokka: rapid prokaryotic genome annotation. Bioinformatics. 30,
955 2068–2069. https://doi.org/10.1093/bioinformatics/btu153
956 55. Simão, F.A., Waterhouse, R.M., Ioannidis, P., et al., 2015. BUSCO: assessing genome
957 completeness. Bioinformatics. 31, 3210–3212.
958 https://doi.org/10.1093/bioinformatics/btv351
959 56. Sokal, R.R., Sneath, P.H.A., 1963. Principles of Numerical Taxonomy. W.H. Freeman,
960 San Francisco, USA.
961 57. Soler-Rivas, C., Jolivet, S., Arpin, N., et al., 1999. Biochemical and physiological
962 aspects of brown blotch disease of *Agaricus bisporus*. FEMS Microbiol. Rev. 23, 591–
963 614. https://doi.org/10.1111/j.1574-6976.1999.tb00415.x
964 58. Stamatakis, A., 2014. RAxML version 8: a tool for phylogenetic analysis and post-
965 analysis of large phylogenies. Bioinformatics. 30, 1312–1313.
966 https://doi.org/10.1093/bioinformatics/btu033
967 59. Suyama, K., Negishi, H., Wakimoto, S., 2000. Selective medium for isolation of
968 *Pseudomonas tolaasii*, the causal bacterium of bacterial blotch of cultivated
969 mushrooms. J. Agric. Sci. 44, 295–301.
970 60. Taparia, T., Krijger, M., Haynes, E., et al., 2020. Molecular characterization of
971 *Pseudomonas* from *Agaricus bisporus* caps reveals novel blotch pathogens in Western
972 Europe. BMC Genomics. 21, 1–15. https://doi.org/10.1186/s12864-020-06905-3
973 61. Tettelin, H., Riley, D., Cattuto, C., et al., 2008. Comparative genomics and the bacterial
974 pan-genome. Curr. Opin. Microbiol. 11, 472–477.
975 https://doi.org/10.1016/j.mib.2008.09.006
976 62. Thomassen, G.M.B., Reiche, T., Tennfjord, C.E., et al., 2022. Antibiotic resistance
977 among *Pseudomonas* in salmon processing environments. Microorganisms. 10, 1420.
978 https://doi.org/10.3390/microorganisms10071420
979 63. Van Belkum, A., Sluijter, M., de Groot, R., et al., 1996. Novel BOX-PCR assay for
980 high-resolution typing of *Streptococcus pneumoniae* strains. J. Clin. Microbiol.
981 34,1176–1179. https://doi.org/10.1128/jcm.34.5.1176-1179.1996
982 64. Wang, Y., Dong, W., Xiang, K., Wang, Q., He, L., Sheng, X., 2021. A combination of
983 genomics, transcriptomics, and genetics provides insights into the mineral weathering

984 phenotype of *Pseudomonas azotoformans* F77. Appl. Environ. Microbiol. 87, e01552-
985 21. https://doi.org/10.1128/AEM.01552-21
986 65. Wells, J.M., Sapers, G.M., Fett, W.F., et al., 1996. Postharvest discoloration of the
987 cultivated mushroom *Agaricus bisporus* caused by *Pseudomonas tolaasii*, *P.*
988 *"reactans*," and *P. "gingeri*". Phytopathology. 86, 1098–1104.
989 https://doi.org/10.1094/Phyto-86-1098
990 66. Wiemann, P., Sieber, C.M.K., von Bargen, K.W., et al., 2013. Genome-wide analyses
991 of *Fusarium fujikuroi* reveal complex regulation of secondary metabolism and novel
992 metabolites. PLoS Pathog. 9, e1003475. https://doi.org/10.1371/journal.ppat.1003475
993 67. Wong, T., Ly-Trong, N., Ren, H., et al., 2025. IQ-TREE 3: phylogenomic inference
994 software using complex evolutionary models. Preprint.
995 https://doi.org/10.32942/X2P62N
996 68. Wong, W.C., Fletcher, P.T., 1979. Identification of *Pseudomonas tolaasii*: the white
997 line in agar and mushroom tissue block rapid pitting tests. J. Appl. Bacteriol. 47, 401–
998 407. https://doi.org/10.1111/j.1365-2672.1979.tb01200.x
999 69. Xiang, Q., Dong, W., Zheng, X., & Sheng, X. (2025). Integrated physiological and
1000 metabolomic analysis reveals the cytochrome c oxidase gene *ccoQ*-mediated biotite
1001 dissolution by *Pseudomonas pergaminensis* F77. Chem. Geol. 694, 123020.
1002 https://doi.org/10.1016/j.chemgeo.2025.123020.
1003 70. Young, J.M., 1970. Drippy gill: a bacterial disease of cultivated mushrooms caused by
1004 *Pseudomonas agarici* sp. nov. N. Z. J. Agric. Res. 13, 977–990.
1005 https://doi.org/10.1080/00288233.1970.10430530
1006 71. Zhang, M., Zhao, L., Tang, F., Gao, J.-M., & Qi, J. (2024). Chemical structures,
1007 biological activities, and biosynthetic analysis of secondary metabolites from *Agaricus*
1008 mushrooms: a review. J. Agric. Food Chem. 72, 12387–12397.
1009 https://doi.org/10.1021/acs.jafc.4c01861

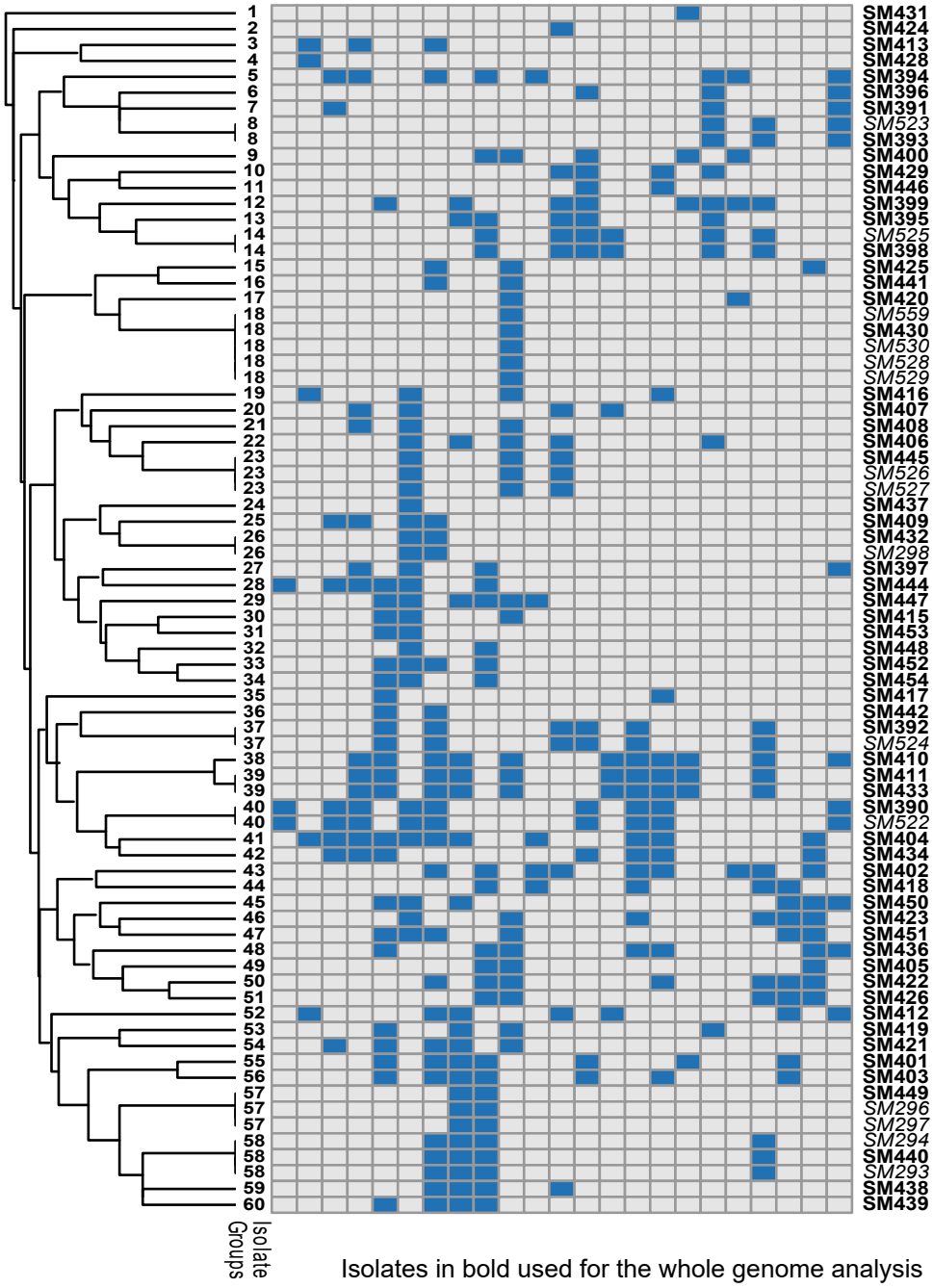

Supplementary Figure 1. Genetic diversity of *Pseudomonas* isolates based on BOX-PCR profiles. BOX-PCR fingerprinting of 77 bacterial isolates produced banding patterns on agarose gel. A binary data matrix, constructed from the presence or absence of 23 distinct BOX-PCR bands, was used for clustering analysis. The resulting dendrogram revealed 60 clusters at a 90% similarity threshold. Based on these DNA fingerprinting patterns, 15 strains with identical BOX-PCR profiles were isogenic and excluded from further analyses. Isolates shown in bold were selected for whole-genome sequencing.